*Key Engineering Materials*
*ISSN: 1662-9795, Vol. 1057, pp 81-87*
*doi:10.4028/p-Q9p090*

*Submitted: 2025-09-22*
*Revised: 2025-12-21*
*Accepted: 2026-02-26*
*Online: 2026-05-21*

# Body Diode Reliability and Reverse Recovery Characteristics of Short Tapered SJ-MOSFET Fabricated by MeV Al Ion Implantation

Takeshi Tawara[1,a*], Kensuke Takenaka[1,b], Syunki Narita[2,c] and Shinsuke Harada[1,d]

[1]National Institute of Advanced Industrial Science and Technology (AIST), Tsukuba West, 16-1 Onogawa, Tsukuba, Ibaraki 305-8569, Japan

[2]Fuji Electric Co., Ltd., 4-18-1 Tsukama, Matsumoto, Nagano 390-0821, Japan

[a*]tawara-takeshi@aist.go.jp, [b]takenaka-kensuke@aist.go.jp, [c]narita-syunki@fujielectric.com, [d]s-harada@aist.go.jp

**Keywords:** superjunction, MeV implantation, body diode, reverse recovery.

**Abstract.** MeV-SJ-MOSFET with short tapered SJ columns was developed by high-energy (MeV) Al ion implantation and was evaluated for the reverse recovery characteristics and the body diode reliability compared to those of Multiepi-SJ. MeV-SJ alleviated the increase in on-resistance at elevated temperatures regardless of short SJ columns and exhibited soft reverse recovery characteristics due to the short tapered SJ shape. MeV-SJ also suppressed the body diode degradation more than Multiepi-SJ. It was considered that the carrier lifetime of drift layer of MeV-SJ may be decreased by non-radiative defects.

## Introduction

A 1.2kV SiC semi-SJ-MOSFET formed by multi-epi process (repetition of epitaxial growth and ion implantation of medium-energy (keV)) has advantages of a low specific on-resistance ($R_{on}A$), soft reverse recovery and suppression of bipolar degradation of the body diode even at a high temperature [1-3]. However, due to the low diffusion coefficients of dopant atoms, the cost of Multiepi process is relatively high because of a large repetition number [4]. Recently MeV ion implantation process (deep ion implantation at MeV energies) was proposed to address the cost issue [5,6], but there are no detailed studies. In this study, we investigated the reverse recovery and bipolar degradation of the body diode of SJ-MOSFET formed by the MeV ion implantation process.

## Experiment

N-type epitaxial layers were grown on a 4H-SiC commercial substrate, followed by Al ion implantation at room temperature (R.T.) up to 8.0 MeV to form the SJ structure. A trench-MOSFET with 2.5 μm depth short tapered p-columns (MeV-SJ) was fabricated. The tapered shape was employed to enhance the soft reverse recovery. For comparison, a trench-MOSFET (UMOS) and a trench-MOSFET with 5.2 μm depth SJ columns formed by multiepi method (Multiepi-SJ) were also fabricated. MeV-SJ and Multiepi-SJ have an identical design of the drift epitaxial layers. Cross-sectional schematics and SEM micrographs of devices are illustrated in Figs. 1 and 2, respectively. The fabricated devices were mounted in TO-247 PKG, and their static and dynamic characteristics were evaluated. Reverse recovery characteristics were evaluated using a double pulse test method, where the same type of devices were used for the MOSFET and the body diode. The load inductance was 1mH, the gate resistance was 75 Ω and the junction temperature was 175 °C. Then we evaluated bipolar degradation of the body diode under a maximum current stress of 1500 A/cm$^2$ for 5 min at 175 °C. Finally, implantation defects were investigated by cathodoluminescence (CL) at 28 K [7].

## Results & Discussion

### 1. Static characteristics

Typical static characteristics at R.T. and 175 °C are summarized in Table. 1. Blocking waveforms are displayed in Fig. 3. MeV-SJ has a lower breakdown voltage for the shorter SJ columns than Multiepi-SJ, but shows a stable avalanche breakdown. Temperature dependences of specific on-resistance ($R_{on}A$) are presented in Fig. 4. Multiepi-SJ and MeV-SJ show lower $R_{on}A$ and weaker temperature dependence than UMOS, which originates from the high doping density of their drift layers.

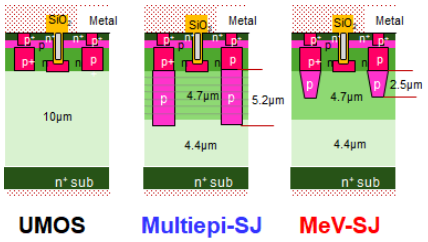


**Fig. 1.** Cross-sectional schematics of devices.

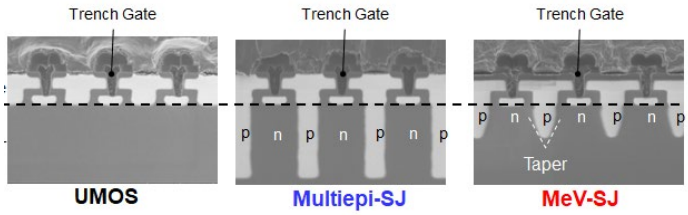


**Fig. 2.** Cross-sectional SEM micrographs of devices.

**Table I.** Typical static characteristics.

| | UMOS | | Multiepi-SJ | | MeV-SJ | |
|---|---|---|---|---|---|---|
| | RT | 175°C | RT | 175°C | RT | 175°C |
| Die sizes | 3.0 x 3.0 $mm^2$ | | 3.0 x 3.0 $mm^2$ | | 3.0 x 3.0 $mm^2$ | |
| BV (V, @Id=4e-5A) | 1566 | 1527 | 1585 | 1607 | 1128 | 1157 |
| $V_{th}$ (V, @Id=18mA) | 3.4 | 2.1 | 3.9 | 2.5 | 4.1 | 2.7 |
| $R_{on}A$ (mΩ $cm^2$, @Vgs=20V) | 3.3 | 6.5 | 3.1 | 4.5 | 3.0 | 4.1 |

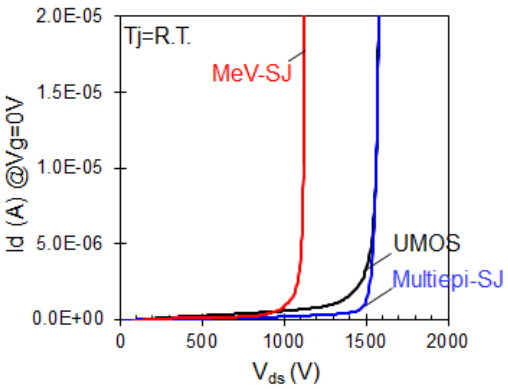


**Fig. 3.** Blocking waveforms.

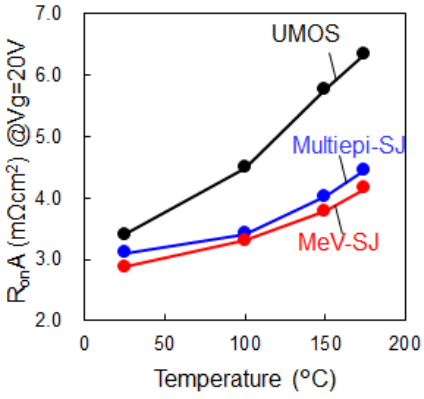


**Fig. 4.** Temperature dependences of Specific on-resistance.

### 2. Reverse recovery characteristics

First, we investigated the effect of the shape of SJ columns on the reverse recovery characteristics. The reverse recovery waveforms of 1.2kV class SJ-MOS were simulated by Sentaurus TCAD simulation for the two SJ column shapes (SJ-straight and SJ-taper) and UMOS in the chopper circuit where the same type of devices were used in MOS and body diode. The results are depicted in Fig. 5. SJ-straight show large dV/dt and dir/dt values, while SJ-taper shows smaller values. In SJ devices, the dir/dt drastically changes when the output capacitance ($C_{oss}$) rapidly decreases due to the full

depletion of SJ columns [8,9]. The tapered shape of SJ columns alleviates the abrupt change of $C_{oss}$ caused by the pinch-off of SJ columns, resulting in the soft recovery waveform.

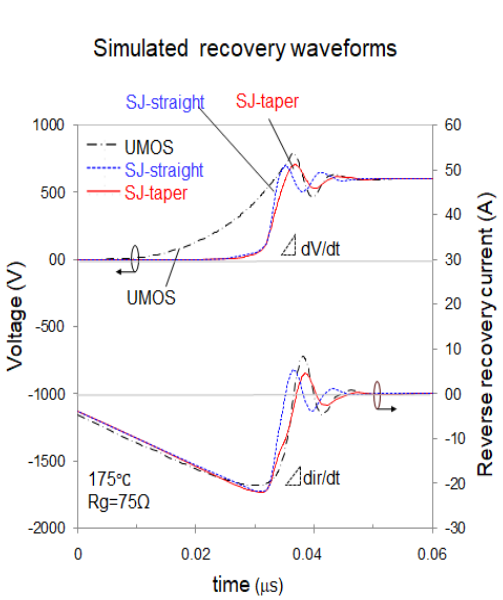


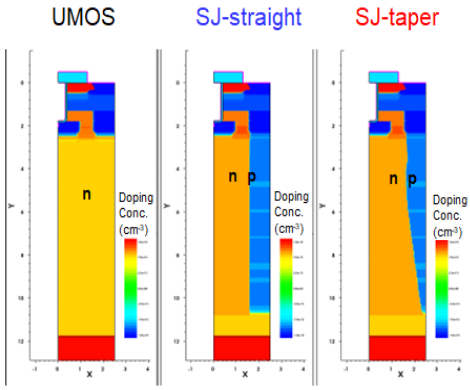


| | Maximum dV/dt (kV/μs) | Maximum dir/dt (kA/μs) | BV @R.T. (V) | $R_{on}A$ @175°C (mΩcm²) |
|---|---|---|---|---|
| UMOS | 55 | 10 | 1575 | 5.70 |
| SJ-straight | 300 | 9 | 1694 | 4.69 |
| SJ-taper | 173 | 6 | 1564 | 4.39 |

**Fig. 5.** Simulated reverse recovery waveforms of devices with different SJ column shapes.

Second, we present the measured reverse recovery waveforms in Fig 6. MeV-SJ presents soft recovery waveforms by the short tapered columns. Then the current dependences of reverse recovery charge ($Q_{rr}$) are shown in Fig. 7. The dependence for MeV-SJ is very weak, indicating that the carrier injection is suppressed at elevated temperatures similar to Multiepi-SJ. The smaller $Q_{rr}$ value of MeV-SJ arises from the small junction capacitance for short SJ columns. The measured $C_{oss}$–$V_{ds}$ characteristics are presented in Fig. 8 (a). MeV-SJ exhibits small $C_{oss}$ without second sharp decline caused by the pinch-off of SJ columns. The simulated $C_{oss}$-$V_{ds}$ curves in Fig. 8 (b) are in good agreement with the measured $C_{oss}$-$V_{ds}$ curves. The depletion layer at $V_{ds}$ of 20, 50 and 120 V are depicted in Fig. 8 (c). The depletion layer of Multiepi-SJ is expanding laterally and pinched off causing the drastic change of $C_{oss}$ at around 100 V while that of MeV-SJ is expanding vertically, which leads to the gradual change of $C_{oss}$.

Then the turn-on and turn-off waveforms of each device are presented in Fig. 9 and 10, respectively. The dV/dt of MeV-SJ is also smaller than that of Multiepi-SJ and there are no clear differences in Turn-off waveforms.

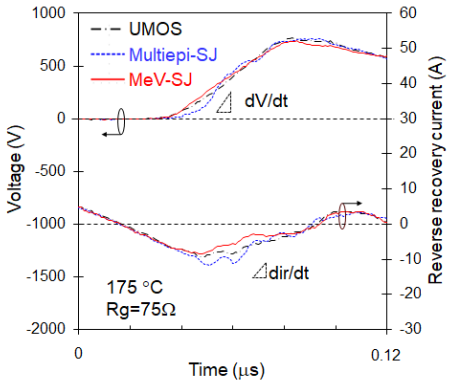


**Fig. 6.** Reverse recovery waveforms at 175 °C.

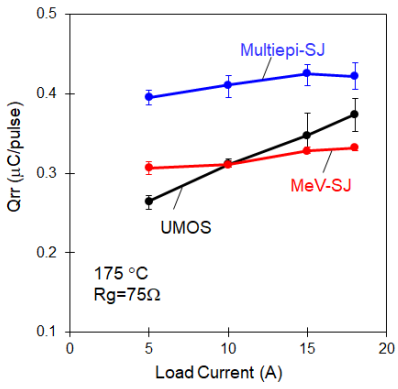


**Fig. 7.** $Q_{rr}$ dependencies on load current.

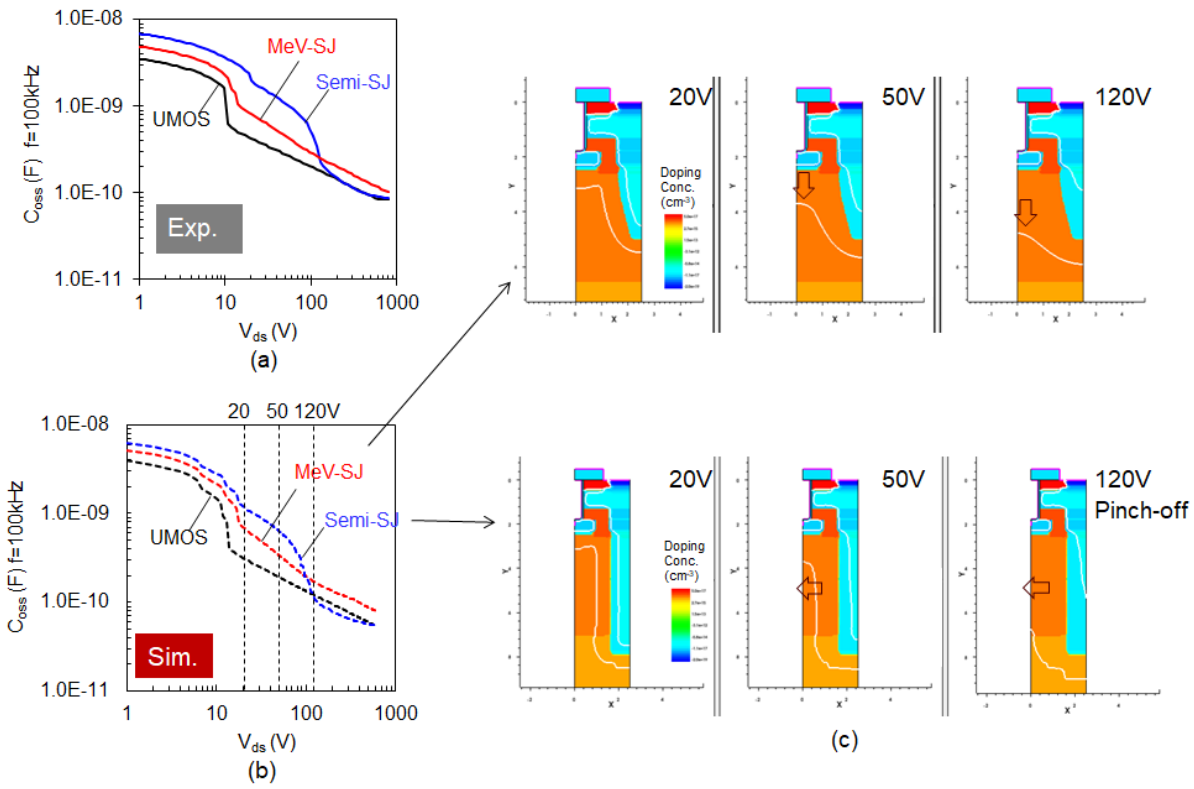


**Fig. 8.** (a) Measured and (b) simulated Output capacitance characteristics and (c) the depletion layer of each device.

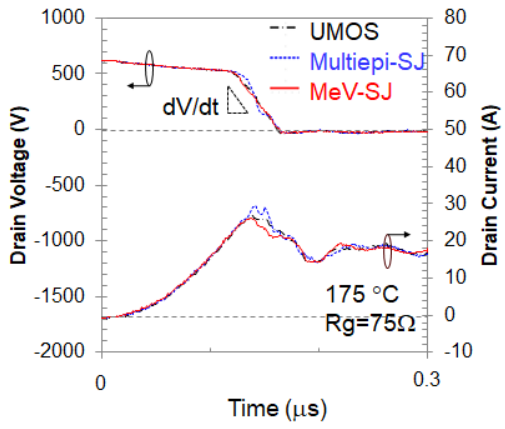


**Fig. 9.** Turn-on waveforms.

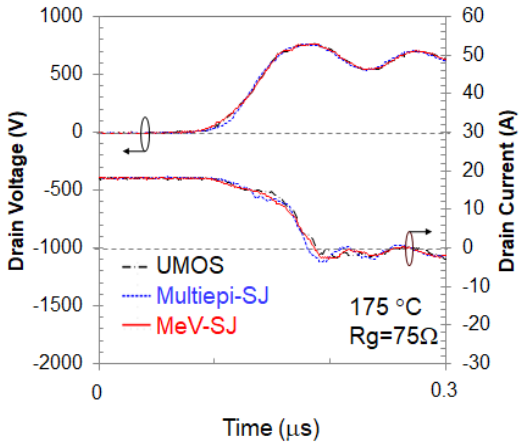


**Fig. 10.** Turn-off waveforms.

## 3. Body diode reliability

Body diode reliability was evaluated with the current stress test up to 1500 A/cm$^2$ at 175 °C. The $V_f$ variations after each current stress are presented in Fig. 11. MeV-SJ shows higher durability than Multiepi-SJ. We observed the PL image with a wavelength of 420 nm after the 1500 A/cm$^2$ stress test. Most devices show the bar-shaped single Shockley Stacking Faults (bar-shaped SFs) in chips. The typical width of bar-shaped SFs is 60 μm in Multiepi-SJ and 30 μm in MeV-SJ. Those values equivalent to the depth of 4 μm and 2 μm considering the substrate off-angle of 4 °. Bar-shaped SFs of MeV-SJ are assumed to stop expanding in the buffer layer.

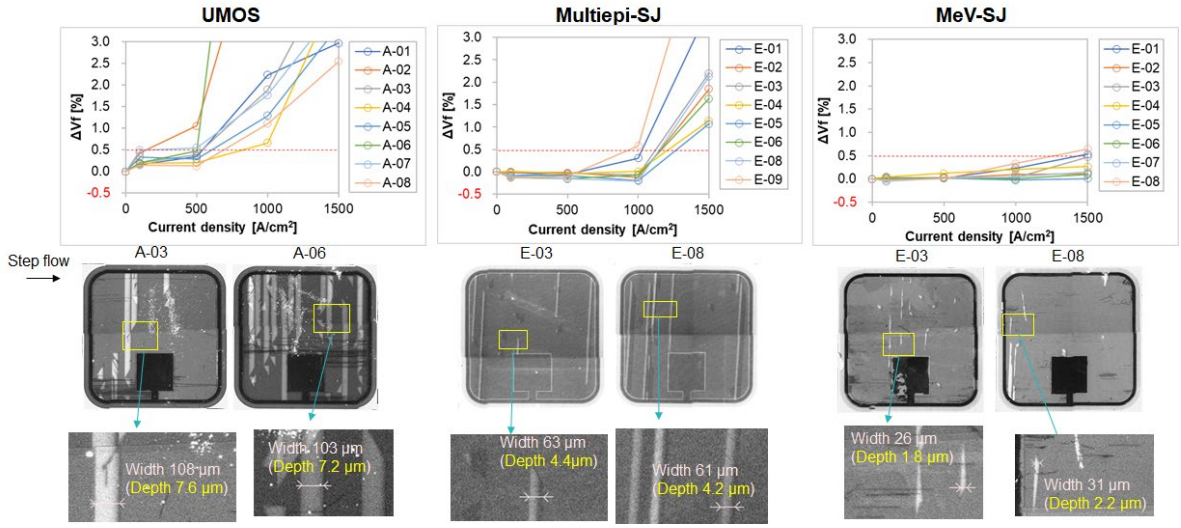


**Fig. 11.** (Upper) $\Delta V_f$ dependences on current stress and (Lower) PL images ($\lambda = 420 \pm 5$ nm) after the current stress of 1500 A/cm$^2$.

The simulated hole density profile of MeV-SJ under the current stress of 1500 A/cm$^2$ at 175 °C is presented in Fig. 12 where the carrier lifetime of both drift layer consisting of SJ columns and buffer layer is changed from 1 ns to 100 ns. As described in Ref. 7, the Al implantation to form SJ columns decreases a carrier lifetime in the drift layer. In Fig. 12, the dotted line indicates the expansion threshold of bar-shaped SFs at the buffer/substrate interface as reported in Ref. 10, which is 1e16 cm$^{-3}$. If the hole density exceeds the threshold, bar-shaped SF would expand from epi/substrate interface. In the case of the lifetime of 1ns, there is no region of hole density over the threshold near the epi/substrate interface and no bar-shaped SFs would expand. On the other hand, for the lifetime of 100 ns, the hole density exceeds the threshold in the whole drift layer and a bar-shaped SF would expand to the surface. However, in the case of the lifetime of 5 and 7.5 ns, there is a local region of hole density under the threshold. A bar-shaped SF expanding from epi/substrate interface would stop at the region and become narrow as reported in Ref. 11. The region of high hole density near the epi/substrate interface is supported by the excess electron injection into the buffer region from the substrate side and extends with increasing the drift layer lifetime. From these results, the lifetime in drift region of MeV-SJ would be smaller than that of Multiepi-SJ.

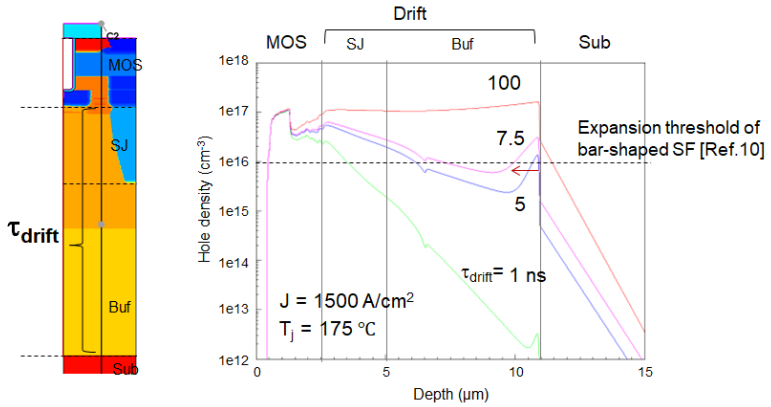


**Fig. 12.** Simulated hole density profile of devices with different lifetimes of drift layer.

Finally, we investigated ion implantation defects using CL imaging. First the typical CL spectra are presented in Fig. 13(a). CL spectrum of Multiepi-SJ and MeV-SJ have different intensities but similar peaks in each device region. The cross-sectional images of the $L_1$ line which is a well-known implantation defect, are shown in Fig. 13 (b). The intensity is standardized by the near the band edge intensity. The $L_1$ intensity of Multiepi-SJ is stronger than that of MeV-SJ in SJ and buffer region.

This would be caused by the extensive thermal history of Multiepi-SJ where the epitaxial growth is repeated. The $L_1$ line intensity is reported to increase under high-temperature annealing [12]. On the other hand, these results cannot explain the higher body diode reliability of MeV-SJ. The non-radiative defects that are not detected in CL may affect the suppression of bipolar degradation.

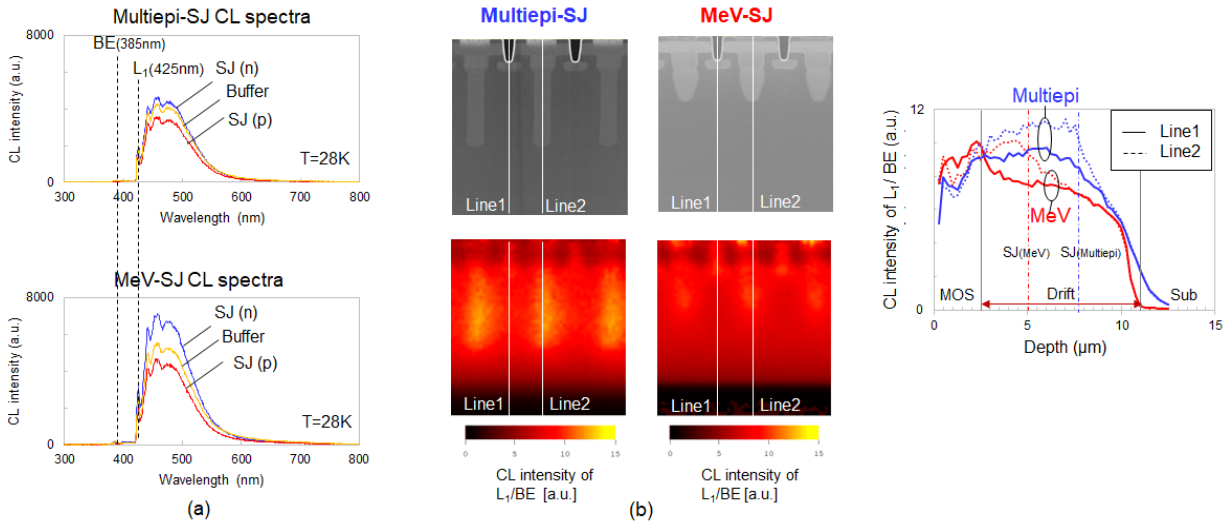


**Fig. 13.** (a) CL spectra of devices. (b) Cross-sectional SEM micrographs and CL images of normalized $L_1$ line luminescence and those line profiles.

## Summary

Even short SJ columns of 2.5 μm can mitigate the increase of on-resistance at high temperatures because of high doping concentration of the drift layer. Short tapered SJ columns soften the reverse recovery waveform by mitigating the abrupt change of $C_{oss}$. MeV-SJ suppresses the body diode degradation more than Multiepi-SJ due to the short carrier lifetime of the drift region. MeV-SJ with short tapered SJ columns has the advantage of high reliability of the body diode and soft reverse recovery compared with Multiepi-SJ.

## Acknowledgement

This study was implemented under a joint research project of Tsukuba Power Electronics Constellations (TPEC). Specifically, T. Tawara and K. Takenaka were assigned from Fuji Electric Co., Ltd. Authors specially thanks to Mr. T. Morimoto of AIST and Mr. K. Oozono of PHENITEC SEMICONDUCTOR Corp. for prototyping and helpful discussions.

## References

[1] S. Harada, Y. Kobayashi, S. Kyogoku, T. Morimoto, T. Tanaka, M. Takei, and H. Okumura, IEDM2018 (2018) 181.

[2] Y. Kobayashi, S. Kyogoku, T. Morimoto, T. Kumazawa, Y. Yamashiro, M. Takei, and S. Harada, Proc. ISPSD2019 (2019) 31.

[3] M. Sometani, K. Oozono, S. Ji, T. Morimoto, T. Kato, K. Kojima, and S. Harada, ISPSD2022 (2022) 337.

[4] M. Torky and W. Sung, ICSCRM2024 book of abstracts (2024) 357.

[5] R. Ghandi, C. Hitchcock, S. Kennerly, ICSCRM2024 book of abstracts (2024) 353.

[6] Y. Yonezawa, et al., ICSCRM2023 book of abstracts (2023) 707.

[7] T. Fukui, T. Ishi, T. Tawara, K. Takenaka, and M. Kato, Jpn. J. Appl. Phys. 62 (2023) 016508.

[8] W. Saito, I. Omura, S. Aida, S. Koduki, M. Izumisawa and T. Ogura, Proc. ISPSD2003 (2003) 45.

[9] T. Tawara, K. Takenaka, S. Narita, M. Sometani, K. Oozono, S. Ji, T. Morimoto, and S. Harada, Mat. Sci. in Semiconductor Processing 176 (2024) 108324.

[10] K. Maeda, K. Murata, T. Tawara, I. Kamata, and H. Tsuchida, Appl. Phys. Exp. 12 (2019) 124002.

[11] Y. Yamashiro, M. Okada, M. Baba, T. Tanaka, S. Tomohisa, H. Watanabe, K .Kojima, S. Harada and H. Yamaguchi, Mat. Sci. Forum 1062 (2022) 676.

[12] L. Strasta, F. H. C. Carlsson, S. G. Sridhara, J. P. Bergman, A. Henry, T. Egilsson, A. Hallén, and E. Janzén, Appl. Phys. Lett. 78 (2001) 46.